Electrical, Mechanical and Capacity Percolation Leads to High Performance MoS_2/Nanotube Composite Lithium Ion Battery Electrodes

Yuping Liu,[1#] Xiaoyun He,[2#] Damien Hanlon,[2] Andrew Harvey,[2] Umar Khan,[2] Yanguang Li,[1*] and Jonathan N. Coleman[2**]

[1]*Institute of Functional Nano & Soft Materials (FUNSOM), Jiangsu Key Laboratory for Carbon-Based Functional Materials and Devices, Soochow University, Suzhou 215123, China*

[2]*School of Physics, CRANN and AMBER Centers, Trinity College Dublin, Dublin 2, Ireland*

*yanguang@suda.edu.cn, **colemaj@tcd.ie

[#]These authors contributed equally

Abstract: Advances in lithium ion batteries would facilitate technological developments in areas from electrical vehicles to mobile communications. While 2-dimensional systems like MoS_2 are promising electrode materials due to their potentially high capacity, their poor rate-capability and low cycle-stability are severe handicaps. Here we study the electrical, mechanical and lithium storage properties of solution-processed MoS_2/carbon nanotube anodes. Nanotube addition gives up to $\times 10^{10}$ and ×40 increases in electrical conductivity and mechanical toughness respectively. The increased conductivity results in up to a ×100 capacity enhancement to ~1200 mAh/g (~3000 mAh/cm^3) at 0.1 A/g, while the improved toughness significantly boosts cycle stability. Composites with 20 wt% nanotubes combined high reversible capacity with excellent cycling stability (*e.g.* ~950 mAh/g after 500 cycles at 2 A/g) and high-rate capability (~600 mAh/g at 20 A/g). The conductivity, toughness and capacity scaled with nanotube content according to percolation theory while the stability increased sharply at the mechanical percolation threshold. We believe the improvements in conductivity and toughness obtained after addition of nanotubes can be transferred to other electrode materials such as silicon nanoparticles.

Keywords: percolating, network, anode, mechanical

In recent years, lithium ion batteries (LIBs) have become the most common rechargeable power sources for portable electronic devices and electric vehicles.[1, 2] Nevertheless, they still suffer from several problems; their energy and especially power densities have not fulfilled their ultimate potential while their safety record is not unblemished.[3] A significant problem is that graphite, the dominant anode material used in LIBs, is limited by a relatively low theoretical capacity of 372 mAh/g.[4] As such, the development of the next-generation of LIBs, is expected to see the replacement of graphite-based anodes with alternative materials having higher capacity at similarly low cost. While a range of materials, including silicon, have been envisaged as future LIB anode materials,[4] of particular interest are 2-dimensional (2D) nano-materials[5] such as graphene[6] and MoS_2.[7]

Over the last decade, 2D nano-materials have generated much excitement in the nano-materials science community.[8-10] They come in many types including graphene, transition metal dichalcogenides (TMDs) and transition metal oxides (TMOs). These materials consist of covalently bonded monolayers which can stack *via* van der Waals interactions to form layered crystals.[8, 9] Such 2D nanomaterials are often found as nanosheets with lateral size ranging from 10s of nm to microns and thickness of ~nm.[9] These materials have shown potential for applications[5] in both energy generation[11] and storage.[12]

In the context of LIBs, exfoliated TMDs have received significant attention as prospective anode materials.[13, 14] While bulk MoS_2 was proposed[15] as a Li ion battery electrode material as early as 1980 due to its high capacity and low cost,[14, 16] it never fulfilled its potential due to limited cycle-stability and poor rate capability. It is generally agreed that these factors are caused by the intrinsically poor electrical conductivity of MoS_2,[17] which limits the ability to move charge between Li storage sites and the external circuit. In addition, the lack of mechanical robustness of the resultant electrodes results in cycling-induced mechanical failure. In recent years, enormous efforts have been made to improve the capacity, stability and rate capability of MoS_2 electrodes.[7, 18, 19] One common approach has been the production of composites of MoS_2 and a conductive additive with the aim of enhancing the rate capability. By far the most common approach has been to mix MoS_2 and graphene nanosheets with the aim of enhancing conductivity while retaining the high lithium storage capacity of MoS_2.[20-28] Similar approaches involve mixing MoS_2 with polyaniline nanowires[29] or carbon nanotubes.[19, 30-32]

However, the composite electrodes described above remain far from optimised as LIB electrodes. Although such approaches generally result in good capacity and improved stability, the rate capability is still not as good as had been hoped. In addition, many of the processing techniques used are not straightforward and may not be scalable. Perhaps most importantly, comprehensive compositional studies have not been performed and a detailed understanding of the relationship between nano-conductor content and the electrical or mechanical properties of the electrode is still missing. In fact, even the dependence of electrode capacity on nano-conductor content has not been studied in any depth. We believe that the full optimisation of LIB electrodes based on 2D materials is impossible until such detailed studies have been performed. Moreover, such a study could result in deep insights into the operation of composite electrodes. In addition, any results obtained could probably be transferred to other electrode materials which suffer from poor electrical and mechanical performance.

In this work we have addressed these problems by using MoS_2 as a model system, representing a material with promising lithium storage capacity but poor electrical and mechanical performance. We have carried out a systematic study on composite anodes of MoS_2, produced by liquid phase exfoliation (LPE),[33, 34] mixed with single walled nanotubes (SWNTs). The resultant composites could be formed into electrodes which were highly porous, extremely conductive and mechanically robust.[35] We studied a wide range of electrode compositions observing large increases in electrical conductivity, mechanical toughness and lithium storage capacity. The resultant optimized electrodes demonstrate best in class performance, especially at high rates. Most importantly, we believe the learnings obtained here are general and can be applied to a range of electrode materials.

RESULTS AND DISCUSSION

MoS_2-only anodes

In order to characterize the performance of MoS_2-based films as lithium ion battery anodes, we used LPE to produce dispersions of MoS_2 nanosheets in the solvent N-methyl-pyrrolidone (see methods). This method is extremely versatile and can be used to produce a range of nanosheet types including graphene,[36, 37] MoS_2,[38-40] GaS[41] and black phosphorous.[42, 43] Transmission electron microscopy (TEM) showed the dispersions to contain large numbers of electron transparent, and so relatively thin, nanosheets (Figure 1A, inset). Statistical analysis of the TEM images showed the lateral nanosheet size to vary from ~100 to ~800 nm with a

mean of 332 nm. Measurements of the optical absorbance spectrum (not shown) of the dispersion allowed us to use published metrics[44] to estimate the mean nanosheet length to be ~350 nm, in good agreement with TEM, and a mean nanosheet thickness of ~18 monolayers. This relatively large thickness is a consequence of the centrifugation regime used, which was designed to maximize the total nanosheet mass produced rather than minimize nanosheet thickness.

In order to facilitate subsequent electrode fabrication, the exfoliation product was transferred to water and then lyophilized to give a powder consisting of reaggregated nanosheets as shown in the scanning electron microscope (SEM) image in Figure 1B. Raman spectroscopy (Figure 1C) confirmed the reaggregated material to consist of MoS_2 with no other components visible. This reaggregated material was redispersed in water, mixed with 10% polyacrylic acid (as the binder) and blade coated into Cu foil to form thin films for testing as electrodes. Typically, the electrode loading was ~ 1 mg/cm^2 (~ 4 μm thick) with a typical SEM image of the surface shown in Figure 1D.

These electrodes were characterized electrochemically as lithium ion battery anodes. Figure 1E shows cyclic voltammetry (CV) curves of MoS_2-only electrode for the first three cycles at a scan rate of 0.2 mV/s. During the initial cathodic sweep, the CV curve displays two intense reduction peaks centered at 1.04 V and 0.47 V (versus Li^+/Li, the same hereafter), respectively. The first peak is attributed to the intercalation of Li^+ ions into the layered structure of 2H-MoS_2 and the formation of 1T-Li_xMoS_2, whereas the second peak at 0.47 V is believed to be associated with the conversion reaction of Li_xMoS_2 to metallic Mo and Li_2S.[7] When the potential sweep is reversed anodically, the CV curve exhibits a pronounced oxidation peak centered at 2.33 V, which is typically attributed to the oxidation of Li_2S to S.[7] During subsequent cycles, the two reduction peaks at 1.04 V and 0.47 V disappear and a new peak at 1.63 V emerges. Such a modification in CV curve shape is common to electrode materials based on the conversion reaction mechanism, and reflects permanent structural change during the first cycle. However, the electrochemical response becomes much more reversible in subsequent cycles.

Consistent results were also garnered from galvanostatic charge/discharge experiments. As shown in Figure 1F, the first discharge curve is featured with two obvious plateaus at 1.0~1.1 V and 0.5~0.6 V, respectively. Its corresponding charge curve displays a plateau between 2.1-2.3 V. During the first cycle, the electrode delivers a specific discharge capacity

of 634 mAh/g, and recovers 560 mAh/g upon recharge. The loss in capacity is in line with the irreversible decomposition of the organic electrolyte to form solid electrolyte interface (SEI). We note that for anode materials based on the conversion reaction mechanism, it is well accepted that the first cycle lithiation (discharge) process is distinctively different from that in all subsequent cycles. In particular, it is now established that layered MoS_2 transforms to Mo and Li_2S upon the first discharge. Subsequently, the original layered structure cannot be recovered.[7] The different shapes of the initial discharge curve and 10th or 50th discharge curve are reflective of this permanent structural change (as well as the formation of an SEI layer).

Most importantly, we found that MoS_2 nanosheet electrodes suffer from poor cycling stability. For example, at the specific current of 0.1 A/g, its discharge capacity initiates at >500 mAh/g, but gradually drops to 190 mAh/g over 50 cycles (Fig. 1G). When the specific current is ramped up to 0.5 A/g, the capacity fade becomes more prominent, declining from ~400 mAh/g to <20 mAh/g within 10 cycles. MoS_2-only nanosheets also demonstrate very poor rate capability with negligible capability delivered at 5 A/g and 10 A/g (Fig. 1H).

We can explore the reasons for the gradual failure of these electrodes *via* SEM analysis of the electrode surfaces post cycling (Figure 1I). In this image, the cracking appears to be much more extensive than before cycling. A magnified image (Figure 1J) shows a typical crack which is >200 nm wide and is clearly quite deep. We hypothesize that these cracks formed in response to the expansion/contraction cycles associated with the Li^+ ion insertion/extraction during charge/discharge cycles. Such cracks will have a significant impact on the electrical properties of the electrode and will limit the insertion and extraction of charge.

These results highlight two main problems with networks of MoS_2 nanosheets as lithium ion battery electrodes. Firstly, similar to many papers on MoS_2 nanosheet anodes,[21, 24, 28, 45] the initial capacity of ~400 mAh/g is relatively low compared to values of >1000 mAh/g (at ~ 0.1 A/g) which have been achieved for MoS_2 grown on 3-dimensional graphene current collectors.[20] We believe the major cause of this lower-than-expected capacity lies with the low electrical conductivity of the MoS_2 network.[46, 47] The second problem is associated with the significant fall off in capacity on cycling, particularly at high currents. This is at least partly due to mechanical failure (as evidenced by cracking) due to repeated expansion/contraction cycles. This is likely due to the relatively poor mechanical properties of electrodes both before and after conversion to Li_2S/Mo. Such cracking will result in very poor electrical connectivity within the electrode and will have a pronounced negative impact on the electrode performance.

Thus, it is clear, for networks of nanosheets to display their full potential as battery electrodes, it will be necessary to enhance both their intrinsic electrical and mechanical properties. While a number of papers attempted conductivity enhancement by addition of graphene or nanotubes, no attention has been given to mechanical reinforcement. We believe there are distinct advantages to using carbon nanotubes (CNT) rather than graphene. Firstly, for geometric reasons MoS_2/CNT composites display higher conductivities than MoS_2/graphene composites at equivalent compositions.[48] In addition, we expect nanotubes to provide more effective reinforcement because of their ability to form entangled networks.[49]

MoS_2/SWNT composite films: Composition and Electrical properties

To address this problem, we prepared a range of SWNT/MoS_2 dispersions by solution mixing. These dispersions had nanotube mass fractions in the range 0.1-20wt% (we define mass fraction as $M_f = M_{NT} / (M_{NT} + M_{NS})$ where NT and NS refer to nanotubes and nanosheets respectively). These dispersions were formed into films by vacuum filtration for basic characterization (see Methods). Shown in Figure 2A is an SEM image of such a composite film with 20wt% nanotubes added. It can clearly be seen that the MoS_2 nanosheets are embedded in a network of nanotubes. To confirm the electrode composition, we performed Raman spectroscopy. Shown in Figure 2B is the mean of 100 individual spectra which clearly shows peaks associated with both SWNT and MoS_2 nanosheets. The main nanotube peaks are the radial breathing mode (RBM) at ~170 cm^{-1} and the D and G line at 1344 and 1594 cm^{-1} respectively while the main MoS_2 lines are the E^1_{2g} and A_{1g} at ~380 and 405 cm^{-1} respectively (see inset for magnified view). All of these lines are in their correct positions[50] and no other lines are observed, conforming the films to consist only of MoS_2 and SWNT.

Adding nano-conductors such as carbon nanotubes to an insulating matrix typically results in significant increases in the conductivity of the resulting composite.[51] Recently, a number of papers have described the electrical properties of films consisting of mixtures of exfoliated nanosheets and both nanotubes and graphene.[35, 48, 52] Here, we measured the electrical conductivity of the SWNT/MoS_2 composite films using the four probe technique, plotting the results *versus* M_f in Figure 2C. For the MoS_2-only film, we find an-plane conductivity of ~10^{-6} S/m, close to that reported for similar systems.[35, 46, 48] On addition of nanotubes, the conductivity increases sharply, reaching 1 S/m for 1wt% nanotubes before further increasing to ~10^4 S/m for 20wt% nanotubes.

The increase in conductivity when adding conductors to an insulating matrix is usually described *via* percolation theory.[53] In this framework, at low nanotube loading levels (usually expressed as volume fractions $\phi = V_{NT} / (V_{NT} + V_{NS})$), the conductors form no conducting path through the composite. However, at some critical volume fraction, the electrical percolation threshold, $\phi_{c,e}$, the first conducting path is formed and the composite conductivity increases substantially above that of the matrix. Above the percolation threshold, the composite conductivity is described by the percolation scaling law:[48, 53, 54]

$$\sigma = \sigma_0 \left(\phi - \phi_{c,e}\right)^{t_e} \quad (1)$$

where t_e is the electrical percolation exponent and σ_0 is approximately the conductivity of film prepared from nanotubes alone. As shown in Figure 2D, our data is consistent with percolation theory, with fitting giving values of σ_0=1.1×10^5 S/m, $\phi_{c,e}$=1.9 vol% (*i.e.* 0.7 wt%) and t_e=2.3. This value of σ_0 is consistent with other percolation studies,[35, 48] but also with measurements on nanotubes films showing conductivities of ~10^5 S/m are generally achieved.[55] The percolation threshold is consistent with theory which predicts $\phi_{c,e}$ to be approximately given by the ratio of mean nanotube length to diameter.[54] Such a small percolation threshold for conductivity is useful in a practical sense as only a very small amount of nanotubes can significantly boost the conductivity. This means very little active material must be sacrificed to introduce the conductive paths. Finally the exponent is similar to the universal percolation exponent (n=2.0). We expect these conductivity increases to facilitate fast movement of electrons throughout the electrode and potentially enhance high rate performance.

MoS_2/SWNT composite films: Mechanical properties

While a number of papers have documented the electrical properties of nanosheet/nanoconductor networks,[35, 48] the mechanical properties of such systems have never been studied systematically. Here we describe the mechanical properties of SWNT/MoS_2 composites. To do this, we prepared free standing films of thickness ~75 μm (methods). Representative stress-strain curves are shown in Figure 2E. The MoS_2-only films were mechanically very poor, displaying stiffness, Y, strength, σ_B, strain-at-break, ε_B, and tensile toughness, T, (energy absorbed up to break) values of Y=26±7 MPa, σ_B=0.24±0.06 MPa, ε_B=1.7±0.7% and T=3 kJ/m^3 respectively. These properties are significantly poorer than has been reported for films formed from graphene nanosheets,[56] probably because of the relative small size of the MoS_2 nanosheets used here. This makes it wholly unsurprising that MoS_2-

only films should fail mechanically when subjected to repeated charge/discharge expansion/contraction cycles.

However, as can be seen from Figure 2E, all parameters increase significantly with nanotube content, reaching values of Y=161±46 MPa, σ_B=3.5±0.4 MPa, ε_B=5.2±1% and T=115 kJ/m^3 respectively for the 6 wt% (15 vol%) composite. We note that while the film stiffness and strength increase linearly with nanotube content (dY/dV_f=1.2 GPa and $d\sigma_B/dV_f$=26 MPa), the strain at break and toughness show more interesting behaviour. The strain at break is plotted versus nanotube content in Figure 2F and shows a sharp increase from ~2% to ~4% at a loading of ~1wt%, not far from the electrical percolation threshold. This can be seen much more clearly in the toughness data which is shown in Figure 2G. The toughness does not increase until ~1wt%, after which a sharp and then continuous increase occurs. This behaviour is consistent with mechanical percolation[57-59] where mechanical properties only begin to increase once a filler network has formed. In this case the toughness will depend on the network connectivity and should scale as[57, 58]

$$T = T_{MoS_2} + T_{Net}(\phi - \phi_{c,m})^{t_m} \quad (2)$$

where T_{MoS2} is the toughness of an MoS_2-only film, T_{Net} is a constant which should be similar to the toughness of a nanotube-only network, $\phi_{c,m}$ is the mechanical percolation threshold and t_m is the mechanical percolation exponent. As shown in Figure 2H, our toughness data is consistent with percolation theory, with fitting giving values of T_{Net}=450 kJ/m^3, $\phi_{c,m}$=2.7 vol% (*i.e.* 1.0 wt%) and t_m=0.66. We note that, although percolation of toughness has been suggested for polymer blends,[60] this phenomenon has not been reported for nano-composite systems. The fit value of T_{Net} is within a factor of 4 of previously reported data for nanotube networks,[61] confirming the composite toughness to be dominated by the properties of the network rather than the matrix. In addition, it is worth noting that the mechanical percolation threshold is larger than the electrical threshold: $\phi_{c,m}>\phi_{c,e}$. This is expected as electrical connectivity requires just two inter-nanotube connections per nanotube while mechanical stability of networks requires a minimum of 4 connections on average[62] and so a higher percolation threshold.

That percolation of toughness occurs in SWNT/MoS_2 composite films is of great relevance for battery electrodes for two reasons. Firstly, the dramatically increased toughness means the electrode can absorb much more strain energy without breaking compared to the nanotube-free electrode. This should make the electrode significantly more resilient to the effects of expansion/contraction cycles. Secondly, percolation scaling of any physical property

implies its value to be dominated by the contribution of the percolating network. This means that the contribution of the matrix is unimportant and such toughening should apply both before and after conversion of MoS_2 to Mo/Li_2S. In addition, and perhaps more importantly, it should be possible to toughen a range of other electrode materials such as silicon nanoparticles.[4]

We note that such toughening is probably inherent to the 1-dimensional nature of the nanotubes. This is because such linear structures can entangle,[63] a phenomenon which is very important to the mechanical properties of polymeric systems. This is unlikely to occur when using graphene as a conductive filler. Thus, we believe nanotubes are a superior additive to graphene when it comes to battery electrodes or indeed any application where both electrical and mechanical enhancement is required.

MoS_2/SWNT composite films as Li ion battery anodes

We believe the MoS_2/SWNT composites described above are ideal for fabricating anodes for Li ion batteries. To test this, we produced a set of composite electrodes (0.1 wt%$\leq M_f \leq$20wt%) using exactly the same procedure followed for the MoS_2-only electrodes (see above and methods). Each electrode was subjected to a range of electrochemical testing with the data for the 20wt% composite shown in Figure 3 as an example.

The CV and galvanostatic charge/discharge curves of the composite electrode are shown in Figure 3 A and B and have similar shapes to those of MoS_2-only electrodes, indicative of identical lithiation and delithiation processes. However, the most striking difference between them is that the composite electrode exhibits significantly improved specific capacity and cycling stability. As shown in Figure 3C, the 20wt% composite electrode delivers a remarkable initial capacity of 1281 mAh/g at 0.1 A/g – more than twice larger than that of MoS_2-only electrode, and retains 1215 mAh/g at the end of 50 cycles. Even at 0.5 A/g, a specific capacity of 1146 mAh/g is measured after 50 cycles. Furthermore, the composite electrode is capable of fast charge and discharge (Figure 3D, black circles). At large specific currents of 5 A/g, 10 A/g and 20 A/g, specific capacities of 975 mAh/g, 710 mAh/g and 580 mAh/g are reversibly delivered. These values not only are far superior to the MoS_2-only electrode (grey circles), but also outperform most other MoS_2-based electrode materials as summarized toward the end of this paper. These electrodes are also capable of mid-rate performance which is stable over many cycles. Shown in Figure 3C inset is cycling data for the 20 wt% composite electrode measured

at 2 A/g which shows 81% capacity retention over 500 cycles. This data clearly shows the rate performance of MoS_2-based anodes to be dramatically improved by the addition of nanotubes.

We have summarized the electrochemical performances of all composite electrodes in Figure 4. Shown in Figure 4A-B are data for discharge capacity, measured at two different specific currents, plotted versus cycle number for composites of a subset of mass fractions. Also shown for comparison are data for MoS_2-only and SWNT-only anodes. As described above, the MoS_2-only anodes demonstrate relatively low initial capacity and poor cycling stability, particularly for the 500 mA/g test. However, for both rates, adding nanotubes appears to increase the initial capacity while decreasing the capacity fade after 50 cycles. For example, in the 100 mA/g test, while the capacity of the 0.3wt% composite falls from an initial value of 516 mAh/g to 251 mAh/g after 50 cycles, the equivalent numbers for the 20 wt% composite were 1281 and 1215 mAh/g respectively. We note that this increase in capacity cannot be simply due to the contribution of the added nanotubes (*e.g. via* the rule of mixtures) because the nanotube capacity is relatively small (<200 mAh/g).

The first cycle capacity, $C_{N=1}$, is plotted versus nanotube mass fraction in Figure 4C for both rates. It is clear that $C_{N=1}$ increases dramatically with nanotube content, saturating at ~1250 mAh/g for both rates. This is higher than the values of >1000 mAh/g (at ~ 0.1 A/g) achieved for MoS_2 grown on 3-dimensional graphene current collectors,[20] indicating that adding nanotubes reduces the conductivity-based limitations associated with thick MoS_2 films. Importantly, the capacity after 50 cycles also increases dramatically with nanotube content for both rates as shown in Figure 4D. For the 500 mA/g test, the capacity increased from 8.5 mAh/g for MoS_2 to 1096 mAh/g for the 20 wt% composite, a ×130 increase. For the 100 mA/g test, the increase was from 164 mAh/g for MoS_2 to 1216 mAh/g for the 20 wt% composite, a still impressive ×7.5 increase. We note that, while the capacity is still increasing at a loading level of 20 wt%, the rate of increase is very small and is clearly decreasing with loading level. Thus, we believe the benefits of using nanotubes contents >20wt% are small relative to the economic cost of the extra nanotubes.

Percolation of Capacity

It is clear from the data in Figure 4C that most of the capacity increase occurs around a nanotube content of 1-2 wt%. This is reminiscent of both the conductivity and toughness data (Figure 2) which both show sharp increases at their respective percolation thresholds. In fact, we propose that the growth in capacity as the nanotube content is increased can be described

by percolation theory. Recently, it has been shown that when nanotubes are added to low conductivity MnO_2 supercapacitor electrodes, the capacitance increases in a manner which is consistent with percolation theory.[35] By analogy with this result and in line with previous observations for mechanical percolation,[58] we expect the excess capacity (*i.e.* the capacity increase relative to the MoS_2-only anodes) to scale with nanotube volume fraction according to percolation theory:

$$\Delta C_{N=50} = C_{Perc}(\phi - \phi_{c,c})^{t_c} \quad (3)$$

where $\Delta C_{N=50} = C_{N=50} - C_{N=50}^{MoS_2}$ is the excess capacity, C_{Perc} is a constant, $\phi_{c,c}$ is the threshold of percolation of capacity and n_c is the capacity percolation exponent. We have calculated the excess capacity for each composite electrode and plotted versus $\phi - \phi_{c,c}$ in Figure 4 E-F for the 100 and 500 mA/g tests respectively. Fitting to equation 3 then gives $\phi_{c,c}$ =4.0% for both rates, C_{Perc}=1189±70 mAh/g and t_c=0.16±0.015 for the 100 mA/g test and C_{Perc}=1301±15 mAh/g and t_c=0.19±0.02 for the 500 mA/g test.

The measured capacity percolation threshold, $\phi_{c,c}$, (4 vol%) somewhat higher than both the electrical and mechanical percolation thresholds (1.9 vol% and 2.7 vol% respectively). There are probably three reasons for this. Firstly, the films used for electrical measurements were prepared slightly differently to those used for battery analysis with the latter system containing a small amount of binder. The second reason is associated with the fact that the nanotubes are probably partially oriented in the plane of the film. While the electrical measurements were made in plane, the battery anodes rely on the nanotubes carrying charge from the copper current collector to the lithium storage sites *i.e.* in the out-of-plane direction. In fact, it has been shown that the percolation threshold for aligned rods is higher than that for randomly arranged rods[64] making the difference between $\phi_{c,c}$ and $\phi_{c,e}$ unsurprising. Finally, we note that increasing the capacity requires the nanotube network to extend throughout the electrode and not just span the length of the electrode. This is a more stringent condition making it unsurprising that $\phi_{c,c} > \phi_{c,e}$.

The parameter C_{Perc} has no explicit physical meaning but rather is a measure of the impact of nanotubes on the MoS_2 capacity. This parameter is slightly bigger for the higher rate sample (500 mA/g). This is a reflection of the fact that the resistive nature of the MoS_2-only

electrode is a greater limiting factor at higher rates[35, 65] leaving more scope for improvement on nanotube addition.

The capacity percolation exponent is significantly smaller than the electrical percolation exponent. Similar findings were reported for capacitance percolation in MnO_2/SWNT composite supercapacitors,[35] and recently, percolation of catalytic activity in MoS_2/SWNT composite electrocatalysts.[52] While this is not fully understood, we suggest that the percolative nature of the capacity is due to the scaling of the extent of the interconnected nanotube network with ϕ. When $\phi > \phi_c$, nanotubes can either belong to the network spanning the entire film or be isolated from it. The strength of the network is the probability that a given nanotube belongs to the network and is given by $P \propto (\phi - \phi_c)^{\beta}$.[53] We propose that stronger networks are more able to deliver electrons to lithium storage sites throughout the film. This results in the power law scaling of $\Delta C_{N=50}$ with $\phi - \phi_c$. That the exponent is relatively low may be a reflection of the fact that β is usually quite low. In fact values as low as 0.14 have been proposed for certain lattices.[66] However, it is not clear if the similarity of this β-value and our measured values of n_c is significant or just coincidental.

With this analysis in mind, we can understand the large increase in capacity on nanotube addition as follows. Although MoS_2 can effectively store lithium, this process is only possible if electrons can be supplied to the lithium storage sites. Because of its low conductivity, electrodes of MoS_2 alone can only store lithium in regions where electrons can be supplied effectively *i.e.* in the vicinity of the current collector. However, for MoS_2/SWNT composite electrodes, once the nanotube content exceeds the percolation threshold, there exists an extensive conducting network which connects the current collector to distant parts of the electrode. This allows electrons to be supplied throughout the electrode *via* the network with only a small portion of the journey through the MoS_2. As the nanotube content increases, the fraction of MoS_2 in close proximity of the network increases steadily to the point where electrons can be effectively transported from the current collector to every lithium storage site. Once this has been achieved, further capacity increases will be marginal and the MoS_2 will be able to store lithium at its maximum capacity (see ref[35] for more detailed discussion).

Electrode Stability

Along with poor rate capability, the disappointing cycle-stability is the biggest problem associated with MoS_2 battery electrodes. It appears clear that the expansion/contraction

associated with charge/discharge cycling will result in mechanical degradation of LIB electrodes prepared from brittle materials such as nanosheet networks. We have shown above that addition of nanotubes dramatically improves the toughness of the electrode, reducing the likelihood of mechanical failure. This should have a significant impact on electrode stability. It is clear from the data in Figures 4 A-B that the electrodes become more stable as the nanotube content is increased. For both rates tested, adding nanotubes reduces the degree of capacity fade as the electrodes are cycled.

We can quantify this by plotting the capacity retention, defined as the capacity after 50 cycles divided by the initial capacity, $C_{N=50}/C_{N=1}$, versus nanotube volume fraction as shown in Figure 5A. For both MoS_2-only and the very low M_f composite electrodes, the capacity retention is very low, particularly for the 500 mA/g test. However, for both test rates, we observe a rapid increase in stability at $\phi \approx 2.7$ vol%, a value which is identical to the mechanical percolation threshold. Above this threshold, the capacity retention increases before saturating at values above 90% for the 20 wt% samples. Such high capacity retention is extremely impressive and far superior to most previous MoS_2-based anode materials for lithium ion batteries. The sharp increase in stability at the mechanical percolation threshold strongly implies that the improvement of electrode stability requires the formation of a nanotube network rather than just the addition of nanotubes. This suggests that it is the nanotube network which is stable against charge/discharge. The electrode material is then stabilized by this network.

To explore the stabilization mechanism further, we characterized the 20 wt% MoS_2/SWNT composite anode by SEM before and after 50 charge discharge cycles. Before cycling (Figure 5B) the electrode appeared uniform and largely crack free. However, after cycling (Figure 5C), it was immediately apparent that many cracks had formed over the entire electrode area. However, looking more closely at a typical crack (Figure 5C), many carbon nanotubes can be seen bridging the sides of the crack and acting as electrical connections across the crack. This makes it clear that while addition of nanotubes increases mechanical robustness, it does not necessarily stop crack formation. However, crack prevention is not actually necessary. When crack formation does occur, separating the electrode into a number of islands, the presence of a percolating nanotube network ensures that all MoS_2 nanosheets are in electrical contact with the current collector *via* that network. This ensures continued electrode performance even after many charge/discharge cycles.

It is clear from the data in Figure 4 that both the capacity and stability have saturated by a nanotube loading of 20wt% (40 vol%), making this the optimum composition for MoS_2-based LIB anodes. We can put this data in context by comparing it with literature data for MoS_2-based LIB anodes. The specific capacity of the 20 wt% composite anode is plotted versus the current rate in Figure 6 (filled stars), with literature values for other MoS_2-based electrodes also shown.[25, 27, 28, 30-32, 67, 68] Of all the data collected and presented in this graph, there are only two papers[29, 31] reporting larger specific capacities of (~1300-1400 mAh/g) and only at the low specific current of 100 mA/g. For all rates above 100 mA/g, the 20wt% composite electrode demonstrates outstanding rate capability outperforming all MoS_2-based competitors. For example, at 2 A/g, it displays 1150 mAh/g, 60% higher than its nearest competitor. Even at a high specific current of 10 A/g, it displays ~710 mAh/g, significantly higher than the state of the art.

In addition, we note that the composites studied here have a reasonable density of ~2500 kg/m^3, potentially leading to high volumetric capacity. For example, our best capacity of 1215 mAh/g (0.1 A/g, 50 cycles) corresponds to a volumetric capacity of ~3000 mAh/cm^3, an extremely high value.[4] Given the film thickness of ~4 μm, this leads to an areal capacity of ~1.2 mAh/cm^2. This value compares well with the highest value of areal capacity for silicon nanoparticle anodes of 4.3 mAh/cm^2 reported by Song *et al.*.[69] It is worth noting that the films prepared for mechanical measurements were ~75 μm thick and were still mechanically robust. Assuming diffusions limitations do not become apparent, the ability to achieve thicknesses this high for MoS_2-based electrodes could lead to areal capacities of >20 mAh/cm^2, an extremely large value.

We believe that the role of the nanotube network is to allow the MoS_2 to perform to its full potential. It is worth noting that in all cases above the specific capacity of our composite electrodes were calculated by normalization to the total composite mass. However, if we instead subtract off the NT contribution to the capacity and then renormalize to the MoS_2-only mass, we can find the specific capacity of the MoS_2 in the presence of the nanotube network. This data is shown as the open starts in Figure 6 and varies from 1500 mAh/g at low rate to ~700 mAh/g at 2 A/g current larger than any other MoS_2-based electrodes. These values exceed those of most conversion electrode materials (typically <1000 mAh/g), and approach the practically realizable capacity of Si anodes.[70] We believe that these composites hold great promise as the high-performance anode materials of future lithium-ion batteries.

However, perhaps more importantly, we believe this work demonstrates a clear strategy for maximizing the performance of electrode materials with good lithium storage but poor electrical and mechanical properties. For example, it was recently shown that the performance of silicon nanoparticle anodes could be enhanced by addition of graphene.[71] We believe that replacing the graphene with nanotubes would give significantly greater mechanical reinforcement (due to entanglements) while at least matching the conductivity increases.

CONCLUSION

In conclusion, we have demonstrated high performance MoS_2/SWNT lithium ion battery anodes which demonstrate high capacity, impressive stability and excellent rate performance. These results were achievable because of the presence of the highly conductive SWNT network, which percolates through the MoS_2 nanosheet network, rapidly shuttling electrons to/from all parts of the electrode. This allows the MoS_2-based electrodes to operate effectively, even at very high rates. The nanotube network plays a dual role, also improving the mechanical properties of the electrodes. The dramatically increased toughness of the composites electrodes allows them to withstand the significant expansion/contraction cycles as so dramatically increase the electrode stability and so lifetime. Although some cracking is unavoidable, the presence of the nanotubes mitigates the damage by providing electrical interconnections across the cracks. This ensures no part of the electrode becomes electrically isolated from the rest.

We believe that this work is important, not so much for the demonstration of high performance in MoS_2/SWNT lithium ion battery anodes but because it defines a strategy for maximizing both the capacity and stability of battery electrodes formed from materials with poor electrical and mechanical properties. While the idea of adding nanotubes is not new, this work quantitatively analyzes the effects of the nanotubes on a holistic basis, studying not only capacity and stability but also electrical and mechanical properties. As a result, we have provided insights into the mechanisms of the capacity enhancement. We believe such strategies will be useful to improve the performance of a range of electrode materials with silicon-based anodes[4] the most obvious.

Methods

Materials

Molybdenum(IV) sulphide powder (MoS_2, 99%, CAS 1317-33-5), 1-Methyl-2-pyrrolidinone (NMP, ACS reagent, ≥ 99.0%) and 2-propanol (IPA, LC-MS CHROMASOLV®, ≥99.9%) were obtained from Sigma-Aldrich (Dublin, Ireland). P3-SWNT (CNT, > 90%, contains 1.0-3.0 atomic% carboxylic acid which can be derivatitized with a variety of functional groups.) was purchased from Carbon Solutions, Inc. Whatman Anodisc™ 47 Alumina membranes (pore size 0.2 µm) were obtained from GE Healthcare. Nitrocellulose membrane (hydrophilic, pore size 0.025 µm and 47 mm diameter) were purchased from MF-Millipore membrane. Holey carbon grids (400 mesh) were purchased from Agar Scientific (U.K.).

Preparation of MoS_2 Stock Dispersion

50 mg of MoS_2 in 80 mL of NMP was sonicated for 4 hours using a horn-probe tip sonicator (Sonics Vibra-cell VCX-750W ultrasonic processor) operating at 60 % amplitude. This dispersion was processed in a 100 mL stainless steel metal beaker under ice-cooling. The sonic tip was pulsed for 6 s on and 2 s off to avoid damage to the processor and to reduce solvent overheating. The resultant raw dispersion was placed into three 28 mL of glass vials and then centrifuged for 60 min at 1000 rpm (240 g Hettich Mikro 22 R centrifuge equipped with a fix angle rotor 1016) to remove unexfoliated MoS_2. The sediment was re-used for further exfoliation. The top 20 mL of the dispersion was decanted and subsequently centrifuged for 90 min at 4500 rpm. The sediments from each vial were redispersed in 10 mL of IPA using a sonic bath.

Preparation of MoS_2/SWNT Stock Composites

8 mg of SWNT were added in 80 mL of IPA at a concentration of 0.1 mg/mL and sonicated for 60 min in a horn-probe sonic tip (60% amplitude 750 W processor). Because all dispersions were made in the same solvent it was possible to mix these dispersions to make composite dispersions of any desired mass ratio. This CNT dispersion was then mixed directly with a predetermined concentration of MoS_2 dispersion to form a series of MoS_2/SWNT composites with CNT content spanning from 0-20wt%. The concentration of MoS_2 dispersion was determined by filtration on an alumina membrane and weighting.

Film formation, electrical and mechanical measurements

Equal amount of composite dispersions were filtered onto a nitrocellulose membrane and dried at room temperature. These films were cut into 0.5×2 cm strips and subsequently transferred onto a glass slide using the transfer method of Wu et al.[72]. Electrical conductivity values were calculated from resistivity measurement using a four-point probe technique with a Keithley 2400 source meter (Keithley Instruments, Inc.). It was controlled by a Lab View program (National Instruments, Inc.). The films were also used for Raman spectroscopy and scanning electron microscopy (SEM). The as prepared MoS_2/SWNT hybrid dispersions (with various MoS_2:SWNT ratios) were vacuum filtered onto polyester filter membrane pore size 0.45 μm. The membranes were dried at room temperature and the free standing hybrid films were peeled off. Free standing hybrid films were cut into strips of width ~2.25 mm. Films thicknesses were in the range of 70-80 μm measured using a digital micrometer. N.B. we limited the composites prepared to mass fractions of 6 wt% or less due to the high nanotube masses required to make such thick films. Mechanical measurements were performed using Zwick tensile tester at a strain rate of 0.5 mm/minute. Each data point is an average of 4 measurements.

Characterization

High-resolution SEM images of the prepared MoS_2/SWNT composite materials were obtained using a Zeiss Ultra Plus at an accelerating voltage of 5 kV, with a 30 μm aperture and a working distance of approximately 6 mm. SEM images of the battery electrode films before and after battery cycling were taken on Supera 55 Zeiss scanning electron microscope at an accelerating voltage of 10 kV. Bright-field transmission electron microscopy imaging was performed by using a JEOL JEM-2100 LaB_6 TEM operated at 200 kV. The samples for TEM measurements were suspended in 2-propanol and dropped onto holey carbon grids on a filter membrane to adsorb the excess solvent. Statistical analysis of TEM was preformed of the flake dimensions by measuring the longest axis of each nanosheet and assigning it as the length followed by measuring an axis perpendicular to this at its widest point and assigning it as the width. Raman spectroscopy was performed using a Horiba Jobin Yvon LabRAM HR800 with 532 nm excitation laser wavelength and 10% of maximum laser power (<2 mW). The average spectra were obtained by 100× objective lens (N.A. = 0.8) for each sample and were collected from a 10 μm×10 μm grid extending across the center of each electrode (λ_{ex}=532 nm). The film thickness for electrical conductivity measurement was measured by Dektak 6M profilometry (Veeco Instruments). Step profiles were obtained at five locations on the film and averaged.

Optical extinction spectra were measured on a Varian Cary 5000 in quartz cuvettes with a path-length of 0.4 cm.

Battery Electrode Preparation

The exfoliation products dispersed in IPA were first transferred to H_2O, and lyophilized to form powders. Electrode materials were then mixed with polyacrylic acid (as the binder) in 9:1 weight ratio and dispersed in H_2O to form a homogeneous slurry. Subsequently, the slurry was uniformly applied onto a Cu foil, and vacuum dried at 60^oC for 24 h. The typical loading density of activity materials was about 1 mg/cm^2 (thickness ~ 4 μm). Standard CR 2032 coin cells were assembled in an Ar-filled glovebox by pairing MoS_2 with a piece of Li foil, separated by Celgard 2400 polypropylene membrane and filled with 1 M $LiPF_6$ in 1:1 v/v ethylene carbonate (EC)/dimethyl carbonate (DMC) electrolyte. Galvanostatic charge/discharge tests were conducted in a voltage range of 0.01~3.0 V at different current rates on a MTI Battery Testing System (CT-3008). In addition, cyclic voltammetry curves were collected on CHI 660E potentiostat at a scan rate of 0.2 mV/s.

Acknowledgements: We thank Science Foundation Ireland (11/PI/1087), the European Research Council (SEMANTICS), the European Union Seventh Framework Program under grant agreement n°604391 (Graphene Flagship), the Shanghai Science and Technology Commission, China (Grant No. 13DZ2260900), the National Natural Science Foundation of China (51472173 and 51522208), and the Natural Science Foundation of Jiangsu Province (BK20140302 and SBK2015010320) for financial support. We acknowledge support from the SFI-funded AMBER research centre (SFI/12/RC/2278**)** and the Collaborative Innovation Centre of Suzhou Nano Science and Technology.

Figs

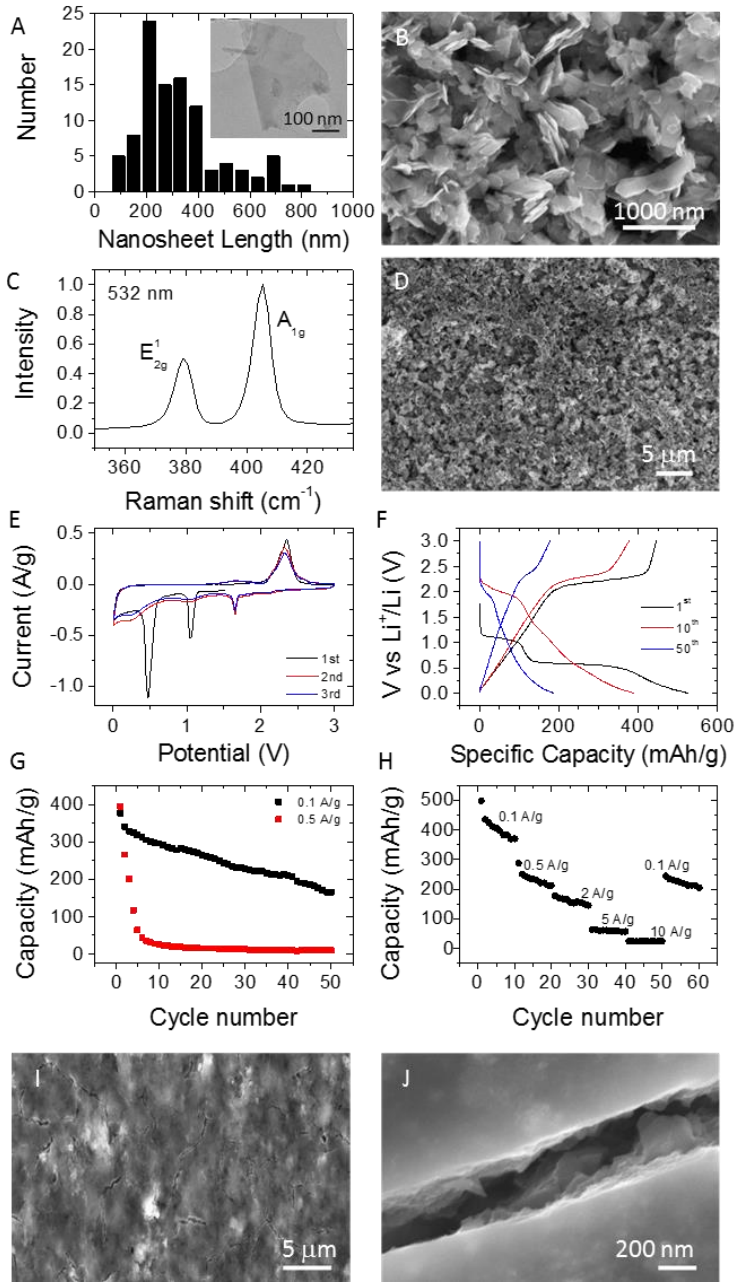

Figure 1: Properties of MoS_2 nanosheet battery electrodes. A) TEM image of a liquid exfoliated MoS_2 nanosheet (inset). Main panel: Histogram of nanosheet length with <L>=332 nm. B) SEM image of reaggregated powder of liquid exfoliated MoS_2 nanosheets. C) Raman spectrum of reaggregated exfoliated MoS_2 nanosheets. D) SEM image of a lithium ion battery electrode fabricated from MoS_2 nanosheets before cycling. E-H) Cyclic voltammetry curves (E), galvanostatic charge-discharge curves (F), capacity versus cycle number (G) and rate capability data (H) for MoS_2 electrodes. I) SEM image of a lithium ion battery electrode fabricated from MoS_2 nanosheets after cycling. J) High magnification image of a crack.

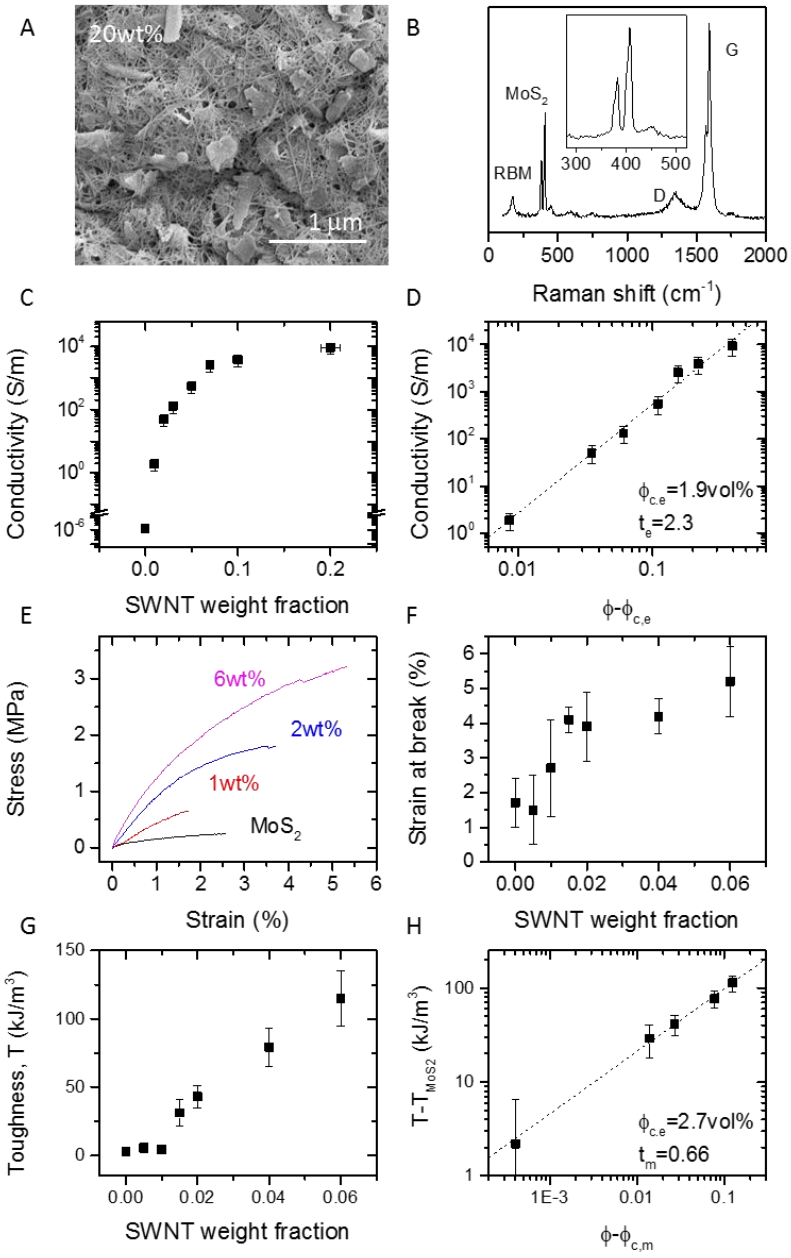

Figure 2: Nanosheet/nanotube composites. A-B) SEM image (A) and Raman spectrum (B) collected from the surface of a film consisting of MoS_2 nanosheets mixed with 20 wt% SWNT. The Raman excitation wavelength was 532 nm. Inset: The MoS_2 peaks are shown more clearly. C) Conductivity of MoS_2/SWNT composite films as a function of SWNT mass fraction. (N.B. there is a break in the conductivity axis.) D) Percolation plot showing film conductivity *versus* ϕ-$\phi_{c,e}$ where ϕ is the SWNT volume fraction and $\phi_{c,e}$ is the electrical percolation threshold. The line is a fit to the percolation scaling law (equation 1). E) Representative stress strain curves for MoS_2/SWNT composite films with different mass fractions. F) Strain at break for

composite films *versus* ϕ. G) Tensile toughness (*i.e.* tensile energy density required to break film) plotted *versus*ϕ. H) Toughness increase relative to MoS_2-only film *versus* ϕ-$\phi_{c,m}$ where $\phi_{c,m}$ is the mechanical percolation threshold. The dashed line is a fit to equation 2.

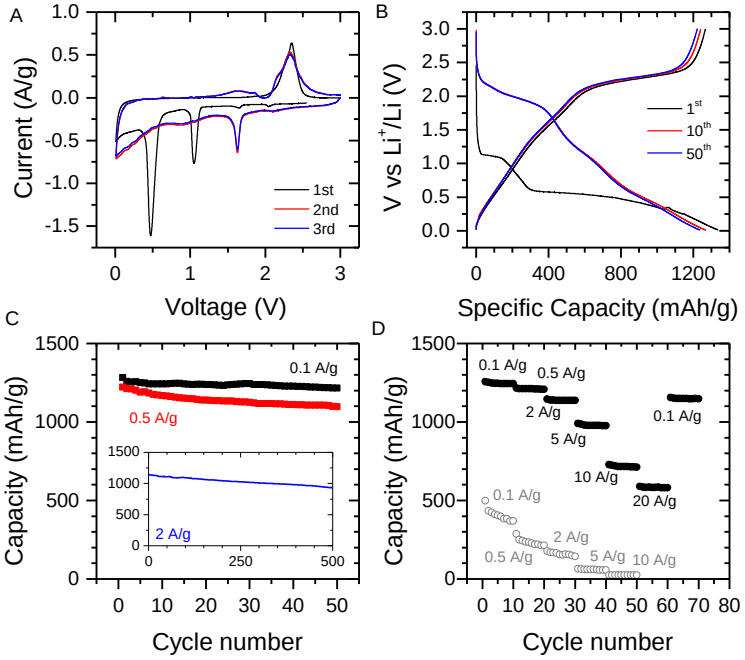

Figure 3: Properties of MoS_2 nanosheet/SWNT composite electrodes (all 20wt%). A) Cyclic voltammetry curves, B), galvanostatic charge-discharge curves, C), capacity versus cycle number and D) rate capability data for MoS_2 electrodes. In D, the grey open circles represent the MoS_2-only data, reproduced from Figure 1.

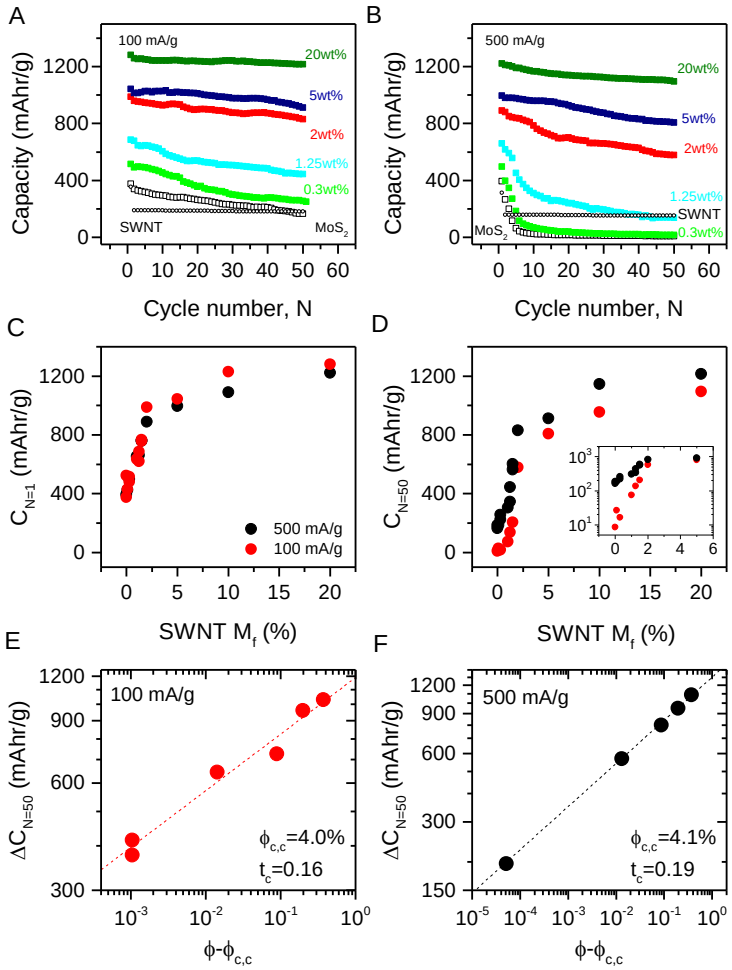

Figure 4: Percolation scaling in composite electrodes. A-B) Capacity versus cycle number for MoS_2/SWNT composite electrodes with a range of SWNT contents. Also shown are equivalent data for SWNT-only and MoS_2-only electrodes. The data in A and B were measured at 100 and 500 mA/g respectively. C-D) Capacity after N=1 (A) and N=50 (B) cycles plotted versus SWNT mass fraction for samples measured at both 100 and 500 mA/g. (D inset): Low mass fraction region of D. E-F) Percolation curves showing the excess capacity (*i.e.* the increase compared to MoS_2-only) after N=50 cycles to scale with nanotube volume fraction according to percolation theory (equation 3) for both the 100 mA/g (E) and the 500 mA/g (F) tests.

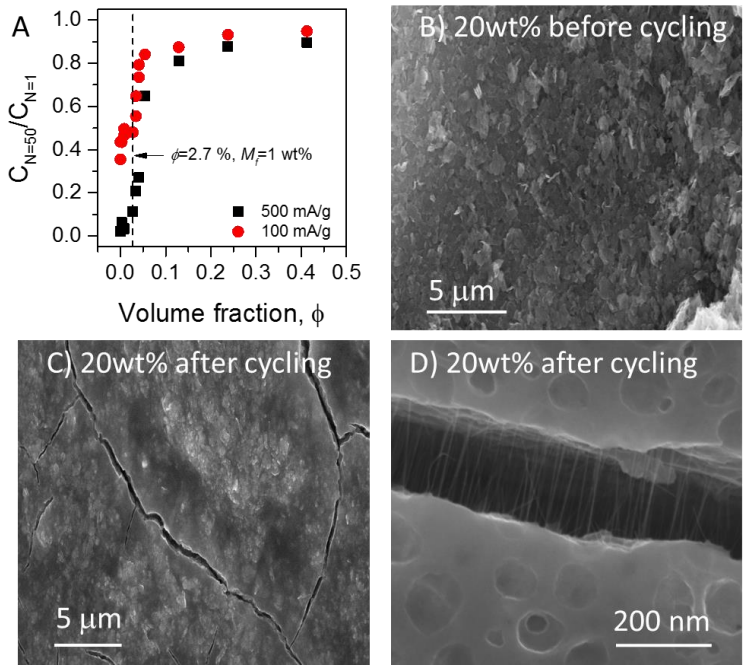

Figure 5: Stabilisation mechanism: A) Capacity retention, defined as ratio of initial capacity to that after 50 cycles, plotted versus SWNT volume fraction for samples measured at both 100 and 500 mA/g. Note that the capacity retention increases sharply at the mechanical percolation threshold ($\phi_{c,m}$=2.7 vol%). B-C) SEM image of the surface of an MoS_2/SWNT (20 wt%) before (B) and after (C) cycling. D) Magnified image of a crack showing bridging by nanotubes.

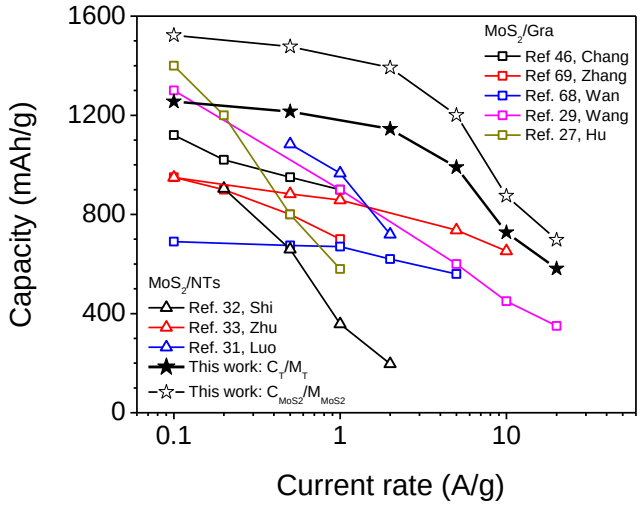

Figure 6: Comparison of the results obtained in this work with comparable data for MoS_2-based electrodes extracted from the literature. The literature data is separated into MoS_2/graphene (squares)[25, 27, 28, 67, 68] and MoS_2/NT (triangles)[30-32] electrodes. The filled stars represent our capacity data (extracted from rate data for the 20 wt% composite), normalised to the total anode

mass. The open stars represent the same data but with the NT contribution subtracted off and the normalised to the MoS_2 mass only.

ToC fig

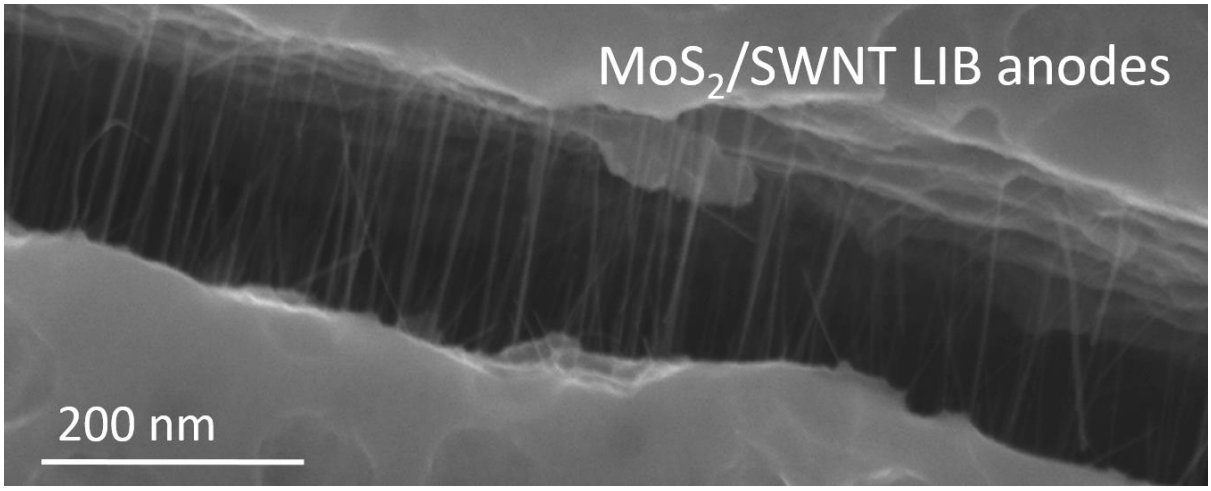

References

1. Kang, K. S.; Meng, Y. S.; Breger, J.; Grey, C. P.; Ceder, G., Electrodes with High Power and High Capacity for Rechargeable Lithium Batteries. *Science* **2006,** 311, 977-980.
2. Choi, N. S.; Chen, Z. H.; Freunberger, S. A.; Ji, X. L.; Sun, Y. K.; Amine, K.; Yushin, G.; Nazar, L. F.; Cho, J.; Bruce, P. G., Challenges Facing Lithium Batteries and Electrical Double-Layer Capacitors. *Angew. Chem.,Int. Ed.* **2012,** 51, 9994-10024.
3. Deng, D., Li-Ion Batteries: Basics, Progress and Challenges. *Energy Sci. Eng.* **2015,** 3, 385-418.
4. Nitta, N.; Wu, F.; Lee, J. T.; Yushin, G., Li-Ion Battery Materials: Present and Future. *Materials Today* **2015,** 18, 252-264.
5. Bonaccorso, F.; Colombo, L.; Yu, G.; Stoller, M.; Tozzini, V.; Ferrari, A. C.; Ruoff, R. S.; Pellegrini, V., Graphene, Related Two-Dimensional Crystals, and Hybrid Systems for Energy Conversion and Storage. *Science* **2015,** 347.
6. Hassoun, J.; Bonaccorso, F.; Agostini, M.; Angelucci, M.; Betti, M. G.; Cingolani, R.; Gemmi, M.; Mariani, C.; Panero, S.; Pellegrini, V.; Scrosati, B., An Advanced Lithium-Ion Battery Based on a Graphene Anode and a Lithium Iron Phosphate Cathode. *Nano Lett.* **2014,** 14, 4901-4906.
7. Stephenson, T.; Li, Z.; Olsen, B.; Mitlin, D., Lithium Ion Battery Applications of Molybdenum Disulfide (Mos2) Nanocomposites. *Energy Environ. Sci.* **2014,** 7, 209-231.
8. Chhowalla, M.; Shin, H. S.; Eda, G.; Li, L.-J.; Loh, K. P.; Zhang, H., The Chemistry of Two-Dimensional Layered Transition Metal Dichalcogenide Nanosheets. *Nature Chem.* **2013,** 5, 263-275.
9. Nicolosi, V.; Chhowalla, M.; Kanatzidis, M. G.; Strano, M. S.; Coleman, J. N., Liquid Exfoliation of Layered Materials. *Science* **2013,** 340, 122641.
10. Wang, Q. H.; Kalantar-Zadeh, K.; Kis, A.; Coleman, J. N.; Strano, M. S., Electronics and Optoelectronics of Two-Dimensional Transition Metal Dichalcogenides. *Nat. Nanotechnol.* **2012,** 7, 699-712.
11. Yang, J.; Shin, H. S., Recent Advances in Layered Transition Metal Dichalcogenides for Hydrogen Evolution Reaction. *J. Mater. Chem. C.* **2014,** 2, 5979-5985.
12. Liu, J.; Liu, X.-W., Two-Dimensional Nanoarchitectures for Lithium Storage. *Adv. Mater.* **2012,** 24, 4097-4111.
13. Balendhran, S.; Walia, S.; Nili, H.; Ou, J. Z.; Zhuiykov, S.; Kaner, R. B.; Sriram, S.; Bhaskaran, M.; Kalantar-zadeh, K., Two-Dimensional Molybdenum Trioxide and Dichalcogenides. *Adv. Funct. Mater.* **2013,** 23, 3952-3970.

14. Gao, M. R.; Xu, Y. F.; Jiang, J.; Yu, S. H., Nanostructured Metal Chalcogenides: Synthesis, Modification, and Applications in Energy Conversion and Storage Devices. *Chem. Soc. Rev.* **2013,** 42, 2986-3017.
15. Haering, R. R.; Stiles, J. A. R.; Brandt, K. Lithium Molybdenum Disulphide Battery Cathode (Us Patent). 1980.
16. Hwang, H.; Kim, H.; Cho, J., Mos2 Nanoplates Consisting of Disordered Graphene-Like Layers for High Rate Lithium Battery Anode Materials. *Nano Lett.* **2011,** 11, 4826-4830.
17. Xiao, J.; Wang, X. J.; Yang, X. Q.; Xun, S. D.; Liu, G.; Koech, P. K.; Liu, J.; Lemmon, J. P., Electrochemically Induced High Capacity Displacement Reaction of Peo/Mos2/Graphene Nanocomposites with Lithium. *Adv. Funct. Mater.* **2011,** 21, 2840-2846.
18. Du, G. D.; Guo, Z. P.; Wang, S. Q.; Zeng, R.; Chen, Z. X.; Liu, H. K., Superior Stability and High Capacity of Restacked Molybdenum Disulfide as Anode Material for Lithium Ion Batteries. *Chem. Commun.* **2010,** 46, 1106-1108.
19. Wang, J.-Z.; Lu, L.; Lotya, M.; Coleman, J. N.; Chou, S.-L.; Liu, H.-K.; Minett, A. I.; Chen, J., Development of Mos2-Cnt Composite Thin Film from Layered Mos2 for Lithium Batteries. *Adv. Energy Mater.* **2013,** 3, 798-805.
20. Cao, X. H.; Shi, Y. M.; Shi, W. H.; Rui, X. H.; Yan, Q. Y.; Kong, J.; Zhang, H., Preparation of Mos2-Coated Three-Dimensional Graphene Networks for High-Performance Anode Material in Lithium-Ion Batteries. *Small* **2013,** 9, 3433-3438.
21. Chang, K.; Chen, W. X., *In Situ* Synthesis of Mos2/Graphene Nanosheet Composites with Extraordinarily High Electrochemical Performance for Lithium Ion Batteries. *Chem. Commun.* **2011,** 47, 4252-4254.
22. Liu, Y. T.; Zhu, X. D.; Duan, Z. Q.; Xie, X. M., Flexible and Robust Mos2-Graphene Hybrid Paper Cross-Linked by a Polymer Ligand: A High-Performance Anode Material for Thin Film Lithium-Ion Batteries. *Chem. Commun.* **2013,** 49, 10305-10307.
23. Wang, Z.; Chen, T.; Chen, W. X.; Chang, K.; Ma, L.; Huang, G. C.; Chen, D. Y.; Lee, J. Y., Ctab-Assisted Synthesis of Single-Layer Mos2-Graphene Composites as Anode Materials of Li-Ion Batteries. *J. Mater. Chem. C.* **2013,** 1, 2202-2210.
24. Zhao, H. H.; Zeng, H.; Wu, Y.; Zhang, S. G.; Li, B.; Huang, Y. H., Facile Scalable Synthesis and Superior Lithium Storage Performance of Ball-Milled Mos2-Graphite Nanocomposites. *J. Mater. Chem. C.* **2015,** 3, 10466-10470.
25. Hu, S.; Chen, W.; Zhou, J.; Yin, F.; Uchaker, E.; Zhang, Q.; Cao, G., Preparation of Carbon Coated Mos2 Flower-Like Nanostructure with Self-Assembled Nanosheets as High-Performance Lithium-Ion Battery Anodes. *J. Mater. Chem. C.* **2014,** 2, 7862-7872.
26. Liu, Y.; Zhao, Y.; Jiao, L.; Chen, J., A Graphene-Like Mos2/Graphene Nanocomposite as a Highperformance Anode for Lithium Ion Batteries. *J. Mater. Chem. C.* **2014,** 2, 13109-13115.
27. Wang, R.; Xu, C.; Sun, J.; Liu, Y.; Gao, L.; Yao, H.; Lin, C., Heat-Induced Formation of Porous and Free-Standing Mos2/Gs Hybrid Electrodes for Binder-Free and Ultralong-Life Lithium Ion Batteries. *Nano Energy* **2014,** 8, 183-195.
28. Chang, K.; Chen, W., L-Cysteine-Assisted Synthesis of Layered Mos2/Graphene Composites with Excellent Electrochemical Performances for Lithium Ion Batteries. *ACS Nano* **2011,** 5, 4720-4728.
29. Yang, L. C.; Wang, S. N.; Mao, J. J.; Deng, J. W.; Gao, Q. S.; Tang, Y.; Schmidt, O. G., Hierarchical Mos2/Polyaniline Nanowires with Excellent Electrochemical Performance for Lithium-Ion Batteries. *Adv. Mater.* **2013,** 25, 1180-1184.
30. Luo, Y.; Zhang, Y.; Zhao, Y.; Fang, X.; Ren, J.; Weng, W.; Jiang, Y.; Sun, H.; Wang, B.; Cheng, X.; Peng, H., Aligned Carbon Nanotube/Molybdenum Disulfide Hybrids for Effective Fibrous Supercapacitors and Lithium Ion Batteries. *J. Mater. Chem. C.* **2015,** 3, 17553-17557.
31. Shi, Y.; Wang, Y.; Wong, J. I.; Tan, A. Y. S.; Hsu, C.-L.; Li, L.-J.; Lu, Y.-C.; Yang, H. Y., Self-Assembly of Hierarchical Mosx/Cnt Nanocomposites ($2 < X < 3$): Towards High Performance Anode Materials for Lithium Ion Batteries. *Sci. Rep.* **2013,** 3.
32. Zhu, C.; Mu, X.; van Aken, P. A.; Maier, J.; Yu, Y., Fast Li Storage in Mos2-Graphene-Carbon Nanotube Nanocomposites: Advantageous Functional Integration of 0d, 1d, and 2d Nanostructures. *Adv. Energy Mater.* **2015,** 5.

33. Coleman, J. N.; Lotya, M.; O'Neill, A.; Bergin, S. D.; King, P. J.; Khan, U.; Young, K.; Gaucher, A.; De, S.; Smith, R. J.; Shvets, I. V.; Arora, S. K.; Stanton, G.; Kim, H.-Y.; Lee, K.; Kim, G. T.; Duesberg, G. S.; Hallam, T.; Boland, J. J.; Wang, J. J., *et al.*, Two-Dimensional Nanosheets Produced by Liquid Exfoliation of Layered Materials. *Science* **2011,** 331, 568-571.
34. Paton, K. R.; Varrla, E.; Backes, C.; Smith, R. J.; Khan, U.; O'Neill, A.; Boland, C.; Lotya, M.; Istrate, O. M.; King, P.; Higgins, T.; Barwich, S.; May, P.; Puczkarski, P.; Ahmed, I.; Moebius, M.; Pettersson, H.; Long, E.; Coelho, J.; O'Brien, S. E., *et al.*, Scalable Production of Large Quantities of Defect-Free Few-Layer Graphene by Shear Exfoliation in Liquids. *Nat. Mater.* **2014,** 13, 624-630.
35. Higgins, T. M.; McAteer, D.; Coelho, J. C. M.; Sanchez, B. M.; Gholamvand, Z.; Moriarty, G.; McEvoy, N.; Berner, N. C.; Duesberg, G. S.; Nicolosi, V.; Coleman, J. N., Effect of Percolation on the Capacitance of Supercapacitor Electrodes Prepared from Composites of Manganese Dioxide Nanoplatelets and Carbon Nanotubes. *ACS Nano* **2014,** 8, 9567-9579.
36. Bourlinos, A. B.; Georgakilas, V.; Zboril, R.; Steriotis, T. A.; Stubos, A. K., Liquid-Phase Exfoliation of Graphite Towards Solubilized Graphenes. *Small* **2009,** 5, 1841-1845.
37. Hernandez, Y.; Nicolosi, V.; Lotya, M.; Blighe, F. M.; Sun, Z.; De, S.; McGovern, I. T.; Holland, B.; Byrne, M.; Gun'ko, Y. K.; Boland, J. J.; Niraj, P.; Duesberg, G.; Krishnamurthy, S.; Goodhue, R.; Hutchison, J.; Scardaci, V.; Ferrari, A. C.; Coleman, J. N., High-Yield Production of Graphene by Liquid-Phase Exfoliation of Graphite. *Nat. Nanotechnol.* **2008,** 3, 563-568.
38. Guardia, L.; Paredes, J. I.; Rozada, R.; Villar-Rodil, S.; Martinez-Alonso, A.; Tascon, J. M. D., Production of Aqueous Dispersions of Inorganic Graphene Analogues by Exfoliation and Stabilization with Non-Ionic Surfactants. *RSC Adv.* **2014,** 4, 14115-14127.
39. Ibrahem, M. A.; Lan, T.-w.; Huang, J. K.; Chen, Y.-Y.; Wei, K.-H.; Li, L.-J.; Chu, C. W., High Quantity and Quality Few-Layers Transition Metal Disulfide Nanosheets from Wet-Milling Exfoliation. *RSC Adv.* **2013,** 3, 13193-13202.
40. Zhou, K.-G.; Mao, N.-N.; Wang, H.-X.; Peng, Y.; Zhang, H.-L., A Mixed-Solvent Strategy for Efficient Exfoliation of Inorganic Graphene Analogues. *Angew. Chem.,Int. Ed.* **2011,** 50, 10839-10842.
41. Harvey, A.; Backes, C.; Gholamvand, Z.; Hanlon, D.; McAteer, D.; Nerl, H. C.; McGuire, E.; Seral-Ascaso, A.; Ramasse, Q. M.; McEvoy, N.; Winters, S.; Berner, N. C.; McCloskey, D.; Donegan, J. F.; Duesberg, G. S.; Nicolosi, V.; Coleman, J. N., Preparation of Gallium Sulfide Nanosheets by Liquid Exfoliation and Their Application as Hydrogen Evolution Catalysts. *Chem. Mater.* **2015,** 27, 3483-3493.
42. Brent, J. R.; Savjani, N.; Lewis, E. A.; Haigh, S. J.; Lewis, D. J.; O'Brien, P., Production of Few-Layer Phosphorene by Liquid Exfoliation of Black Phosphorus. *Chem. Commun.* **2014,** 50, 13338-13341.
43. Kang, J.; Wood, J. D.; Wells, S. A.; Lee, J.-H.; Liu, X.; Chen, K.-S.; Hersam, M. C., Solvent Exfoliation of Electronic-Grade, Two-Dimensional Black Phosphorus. *ACS Nano* **2015,** 9, 3596-3604.
44. Backes, C.; Smith, R. J.; McEvoy, N.; Berner, N. C.; McCloskey, D.; Nerl, H. C.; O'Neill, A.; King, P. J.; Higgins, T.; Hanlon, D.; Scheuschner, N.; Maultzsch, J.; Houben, L.; Duesberg, G. S.; Donegan, J. F.; Nicolosi, V.; Coleman, J. N., Edge and Confinement Effects Allow *in Situ* Measurement of Size and Thickness of Liquid-Exfoliated Nanosheets. *Nature Commun.* **2014,** 5, 4576.
45. Wang, J.; Liu, J.; Luo, J.; Liang, P.; Chao, D.; Lai, L.; Lin, J.; Shen, Z., Mos2 Architectures Supported on Graphene Foam/Carbon Nanotube Hybrid Films: Highly Integrated Frameworks with Ideal Contact for Superior Lithium Storage. *J. Mater. Chem. C.* **2015,** 3, 17534-17543.
46. Cunningham, G.; Hanlon, D.; McEvoy, N.; Duesberg, G. S.; Coleman, J. N., Large Variations in Both Dark- and Photoconductivity in Nanosheet Networks as Nanomaterial Is Varied from Mos2 to Wte2. *Nanoscale* **2015,** 7, 198-208.
47. Cunningham, G.; Khan, U.; Backes, C.; Hanlon, D.; McCloskey, D.; Donegan, J. F.; Coleman, J. N., Photoconductivity of Solution-Processed Mos2 Films. *J. Mater. Chem. C* **2013,** 1, 6899-6904.
48. Cunningham, G.; Lotya, M.; McEvoy, N.; Duesberg, G. S.; van der Schoot, P.; Coleman, J. N., Percolation Scaling in Composites of Exfoliated Mos2 Filled with Nanotubes and Graphene. *Nanoscale* **2012,** 4, 6260-6264.

49. Slobodian, P.; Riha, P.; Saha, P., A Highly-Deformable Composite Composed of an Entangled Network of Electrically-Conductive Carbon-Nanotubes Embedded in Elastic Polyurethane. *Carbon* **2012,** 50, 3446-3453.
50. Murawala, A. P.; Loh, T. A. J.; Chua, D. H. C., Synthesis of Mos2 Nano-Petal Forest Supported on Carbon Nanotubes for Enhanced Field Emission Performance. *J. Appl. Phys.* **2014,** 116.
51. Bauhofer, W.; Kovacs, J. Z., A Review and Analysis of Electrical Percolation in Carbon Nanotube Polymer Composites. *Compos. Sci. Technol.* **2009,** 69, 1486-1498.
52. McAteer, D.; Gholamvand, Z.; McEvoy, N.; Harvey, A.; O'Malley, E.; Duesberg, G. S.; Coleman, J. N., Thickness Dependence and Percolation Scaling of Hydrogen Production Rate in Mos2 Nanosheet and Nanosheet-Carbon Nanotube Composite Catalytic Electrodes *ACS Nano* **2015,** 10, 672-683.
53. Stauffer, D. S.; Aharony, A., *Introduction to Percolation Theory*. 2nd ed.; Taylor & Francis: London, 1985.
54. Bauhofer, W.; Kovacs, J. Z., A Review and Analysis of Electrical Percolation in Carbon Nanotube Polymer Composites. *Composites Science and Technology* **2009,** 69, 1486-1498.
55. Doherty, E. M.; De, S.; Lyons, P. E.; Shmeliov, A.; Nirmalraj, P. N.; Scardaci, V.; Joimel, J.; Blau, W. J.; Boland, J. J.; Coleman, J. N., The Spatial Uniformity and Electromechanical Stability of Transparent, Conductive Films of Single Walled Nanotubes. *Carbon* **2009,** 47, 2466-2473.
56. Ranjbartoreh, A. R.; Wang, B.; Shen, X. P.; Wang, G. X., Advanced Mechanical Properties of Graphene Paper. *J. Appl. Phys.* **2011,** 109, 6.
57. Liff, S. M.; Kumar, N.; McKinley, G. H., High-Performance Elastomeric Nanocomposites *Via* Solvent-Exchange Processing. *Nat. Mater.* **2007,** 6, 76.
58. Nawaz, K.; Khan, U.; Ul-Haq, N.; May, P.; O'Neill, A.; Coleman, J. N., Observation of Mechanical Percolation in Functionalized Graphene Oxide/Elastomer Composites. *Carbon* **2012,** 50, 4489-4494.
59. Kim, H.; Macosko, C. W., Morphology and Properties of Polyester/Exfoliated Graphite Nanocomposites. *Macromolecules* **2008,** 41, 3317-3327.
60. Wu, S. H., A Generalized Criterion for Rubber Toughening - the Critical Matrix Ligament Thickness. *J. Appl. Polym. Sci.* **1988,** 35, 549-561.
61. Blighe, F. M.; Blau, W. J.; Coleman, J. N., Towards Tough, yet Stiff, Composites by Filling an Elastomer with Single-Walled Nanotubes at Very High Loading Levels. *Nanotechnology* **2008,** 19.
62. van Hecke, M., Jamming of Soft Particles: Geometry, Mechanics, Scaling and Isostaticity. *J. Phys. Condens. Matter* **2010,** 22.
63. Rubinstein, M.; Colby, R. H., *Polymer Physics*. First ed.; Oxford University Press: 2003.
64. White, S. I.; DiDonna, B. A.; Mu, M.; Lubensky, T. C.; Winey, K. I., Simulations and Electrical Conductivity of Percolated Networks of Finite Rods with Various Degrees of Axial Alignment. *Phys. Rev. B* **2009,** 79, 024301.
65. Higgins, T. M.; Coleman, J. N., Avoiding Resistance Limitations in High-Performance Transparent Supercapacitor Electrodes Based on Large-Area, High-Conductivity Pedot:Pss Films. *ACS Appl. Mater. Interfaces* **2015,** 7, 16495-506.
66. Sykes, M. F.; Glen, M.; Gaunt, D. S., Percolation Probability for Site Problem on Triangular Lattice. *J. Phys. A: Math. Gen.* **1974,** 7, L105-L108.
67. Wan, Z. M.; Shao, J.; Yun, J. J.; Zheng, H. Y.; Gao, T.; Shen, M.; Qu, Q. T.; Zheng, H. H., Core-Shell Structure of Hierarchical Quasi-Hollow Mos2 Microspheres Encapsulated Porous Carbon as Stable Anode for Li-Ion Batteries. *Small* **2014,** 10, 4975-4981.
68. Zhang, L.; Wu, H. B.; Yan, Y.; Wang, X.; Lou, X. W., Hierarchical Mos2 Microboxes Constructed by Nanosheets with Enhanced Electrochemical Properties for Lithium Storage and Water Splitting. *Energy Environ. Sci.* **2014,** 7, 3302-3306.
69. Song, J.; Zhou, M.; Yi, R.; Xu, T.; Gordin, M. L.; Tang, D.; Yu, Z.; Regula, M.; Wang, D., Interpenetrated Gel Polymer Binder for High-Performance Silicon Anodes in Lithium-Ion Batteries. *Adv. Funct. Mater.* **2014,** 24, 5904-5910.
70. Ma, D. L.; Cao, Z. Y.; Hu, A. M., Si-Based Anode Materials for Li-Ion Batteries: A Mini Review. *Nano-Micro Letters* **2014,** 6, 347-358.
71. Binh Phuong Nhan, N.; Kumar, N. A.; Gaubicher, J.; Duclairoir, F.; Brousse, T.; Crosnier, O.; Dubois, L.; Bidan, G.; Guyomard, D.; Lestriez, B., Nanosilicon-Based Thick Negative Composite

Electrodes for Lithium Batteries with Graphene as Conductive Additive. *Adv. Energy Mater.* **2013,** 3, 1351-1357.
72. Wu, Z.; Chen, Z.; Du, X.; Logan, J. M.; Sippel, J.; Nikolou, M.; Kamaras, K.; Reynolds, J. R.; Tanner, D. B.; Hebard, A. F.; Rinzler, A. G., Transparent, Conductive Carbon Nanotube Films. *Science* **2004,** 305, 1273-1276.